JOURNAL OF COMPUTATIONAL PHYSICS **144,** 358–378 (1998)
ARTICLE NO. CP975824

Grid and Particle Hydrodynamics:

Beyond Hydrodynamics via Fluid Element Particle-in-Cell[1]

William B. Bateson and Dennis W. Hewett

Lawrence Livermore National Laboratory, P.O. Box 808, Livermore, California 94551
E-mail: bateson1@llnl.gov

Received October 25, 1996; revised July 23, 1997

A new plasma/fluid transport algorithm is presented that combines and retains the strengths of the particle and hydrodynamic methods. By including internal velocity characteristics of real particles within each finite size macro-particle (FSP), a redundancy is introduced in the representation of the real particle distribution that is recovered by the superposition of these macro-particles. This redundancy is exploited by merging particles that sufficiently overlap in parameter space. The internal velocity distribution is exploited by allowing the distribution within each FSP to evolve hydrodynamically. In turn the evolution establishes the partitioning of moments into central and expansion particles. Such aggressive increases in the number of individual FSPs probe for emerging features. If interesting features fail to materialize, aggressive merging provides particle economy. The objective is to economically recover details of the particle distribution necessary for accurate collisions. GaPH promises to accomplish this mission without squandering computational resources in uninteresting regions of phase space. This paper reports collisionless GaPH test results that compare well with analytic solutions that initially contain large gradients.

CONTENTS

[1] This work was performed under the auspices of the U.S. Department of Energy by Lawrence Livermore National Laboratory under Contract W-7405-Eng-48 and by Sandia National Laboratory under Contract DE-AC04-94AL85000.

0021-9991/98 $25.00

I. INTRODUCTION

Numerical modeling of the dynamical behavior of fluids or plasmas falls into two broad classes. The first class, fluid or hydrodynamics includes those cases in which the collection of particles are collisional enough to have relaxed to a local drifting Maxwellian. The second class consists of those cases not in the first. In other words, the second class consists of systems in which time scales are so short or the system is so strongly driven that particles making up the system cannot locally be characterized by a drifting Maxwellian.

There are methods to treat the physics in each class. The drifting Maxwellian velocity structures in the first class have been addressed by a wide variety of hydrodynamic or magnetohydrodynamic algorithms. In addition to the fluid drift, the essential features of the velocity distribution are assumed to be represented by a temperature or, perhaps, a pressure tensor that is a function of position. The issues for these methods are often the dynamics of material flow in complex geometries. A principle concern is flow advection; either flow through a computational mesh that entails Eulerian advection or through the Lagrangian motion of the mesh that, in essence, postpones the advection problem until a remapping of the mesh is dictated to preserve mesh element simplicity. Another concern for hydro codes is that, for the problem of turbulence, flows from a variety of spatial locations merge, ultimately within a single mesh cell. When that happens, hydro codes have no alternative but to declare that the net flow within that mesh cell is the simple average and convert the excess energy to temperature. Essential physics is either lost or the user is driven to a prohibitive number of cells.

Systems that cannot be characterized by drifting Maxwellians require "kinetic" codes. Here too, a wide variety of computational methods have arisen to extract the essential physics. The physics now includes the details of the particles' velocity; we now need to know the number of particles $f(\mathbf{x}, \mathbf{v}, t)$ that have (or, equivalently, the probability of finding a particle with) a given velocity at each point in space. The dimensionality that must be modeled has increased to include the required velocity information.

Techniques that have been applied to this "kinetic" problem include: velocity space expansions in orthogonal polynomials (for example, a Hermite velocity expansion recovers a Maxwellian with only one term), full finite-difference or convection scheme which evolves in a finite element representations of both velocity and position space [5] and the particle-in-cell method (PIC) [3]. PIC involves the use of Lagrangian "macro-particles," simply clusters of particles with the equivalent charge over mass, q_s/m_s, that are moved around with finite time steps according to the dictates of $F = ma$. PIC has two tremendous advantages: (1) computer resources are only expended in positions of space that are occupied (compared with grid techniques that must store and integrate even those grid points that have no nearby particles), and (2) the Lagrangian particles have no advection difficulties.

PIC has thus emerged as the method of choice in those systems that are driven hard that have chemical cross sections that are sensitive to population densities on velocity tails, that are susceptible to interpenetration, or that have interacting particle beams. The difficulty with particle methods is expense. Even with the efficiencies of unequally weighted

macro-particles, to adequately represent the details of a chemically significant "bump-on-tail" requires a very large number of particles, most of which ineffectively wander around in the core of the distribution. When the first hint of collisionality occurs, the operations count for PIC skyrockets. Even with null particle collisions [3], the cost for realistic multidimensional simulations becomes prohibitive—certainly not an environment that makes parameter studies enjoyable.

In addition to unequally weighted macro-particles, a variety of other solutions have been proposed. A method called δf has recently gained favor as an economic alternative. The concept is to split the total distribution function $f(\mathbf{x}, \mathbf{v}, t)$ into a fluid core plus particles that each carry a small part of the distribution, hopefully out on the tail where they become a significant or dominant contribution to the total f. This method amounts to a perturbation technique about the core distribution. A difficulty that we have observed is that while the distribution can be initialized with small particles out on the tail, after a finite amount of time, a large fraction of these particles will be found back near the core of the distribution. The issue is that, for strongly nonlinear, driven problems, the birthing and reabsorption of particles must be addressed. The *quiet* PIC method of Barnes and co-workers addresses some of these issues [1].

We propose here a new algorithm that draws from the best features of both PIC and hydrodynamics. A key element of our method derives from confronting the birthing and reabsorption of particles. We allow aggressive increases in the number of "particles" to probe for emerging features and, then with similar aggressiveness, merge particles if interesting structures do not appear. Each "particle" is similar to a macro-particle in some ways and is similar to a small piece of fluid governed by internal hydrodynamics in others ways.

Our concept is similar to the BLOB method [7] of Lapenta and Brackbill who have experimented with particles that have velocity and spatial width. Their collisionless plasma method uses strong electrostatic field gradients to determine if particles should be split and intends to use a coalescing procedure when particle counts get large. In contrast our algorithm aggressively births new particles as a result of fitting individual particle "hydrodynamics" and requires aggressive merging to hold particle numbers in check. Finally, smooth particle hydrodynamics (SPH) [6] and grid and particle (GAP) [2] are also similar to what we propose; both have a Lagrangian push and both have particles with internal structure. However, SPH and GAP do not address birthing and merging issues and require particle shape or a grid for differencing. Our new algorithm has no need for shape or grid-based differencing because these are no equations to spatially difference.

Our method, which we call GaPH for grid and particle hydrodynamics, can be viewed as a natural extension of either PIC or hydrodynamics. In the next section, we discuss these two points of view. In Section III, we give a detailed account of the particle effusion equations and how they are used. In Section VI, we give a few collisionless examples followed by a concluding section.

II. PHILOSOPHY OF GaPH

GaPH is a combination of the best features of PIC and hydrodynamics. More precisely, the philosophy of the GaPH method can be traced to our attempts to improve the deficiencies of these predecessors. Here we discuss the merging of PIC and hydrodynamics from these two points of view.

A. *GaPH as an Extension of PIC*

One of the strengths of PIC is that it handles material advection simply by moving its Lagrangian particles. No upwind, no FCT, no mesh "bowties" to remap. PIC also allows you to spend your computer resources where the material exists and requires only limited resources in vacuum or low density regions. Conversely, simple PIC requires that you spend your computer resources on the material even though the region may be over characterized, such as the core of a Maxwellian. First-order improvements to PIC involve using macro-particles with unequal weights such as using bigger particles in regions that have high density. Unfortunately, while this technique works well early in the simulation, serious stochastic noise problems result when, in strongly nonlinear problems, these large particles wander into low density regions. The GaPH concept addresses these issues by using "smarter" particles that aggressively attempt to make themselves into smaller particles. An added benefit is that these new particles are available to catch and resolve new emerging features—reducing the need to anticipate the location at which new features might emerge. Of course, this formation of new particles must be bounded. GaPH controls the number of particles by aggressive merging in those areas of space in which interesting features fail to materialize. The keys to the method are the formation of new particles and the merging of particles, thus making it feasible to aggressively probe for emerging features.

B. *GaPH as an Extension of Hydrodynamics*

The strength of hydro is its simplicity—all velocity space details are carried by a position dependent flow velocity and temperature (or perhaps a pressure tensor). In cases with sufficient collisionality to make this assumption valid, a vast reduction in dimensionality can be achieved. This allows the user to concentrate on other important issues, such as geometric complexity or radiation. Advection of fluids on a mesh continues to be a problem, with an ever increasing amount of research attempting to find the best advection technique through an Eulerian fixed mesh or how to best control mesh complexity in Lagrangian meshes that move with the fluid.

GaPH approaches this problem by having multiple, perhaps identical, fluid "species" but limiting the spatial extent of each species to the "space" within a single finite size particle (FSP). Each GaPH particle is a spatially isolated piece of fluid which is governed internally by its own hydrodynamics. Of the velocity characteristics, only the bulk flow of this element of hydrodynamics has been removed, now to be treated as the Lagrangian velocity of the center of this FSP. In contrast, typical multiple species hydro methods allow all species the freedom—and mesh allocation—to cover the entire problem domain, with the expectation that fluid quantities will vanish on mesh points where there is no fluid. With GaPH, if there is no density, there will be no GaPH particles. The similarities to ALE codes are obvious; GaPH particles move around like Lagrangian cells. Instead of tracking a grid for each fluid, each fluid element carries its spatial extent and location.

Each finite size GaPH fluid will exhibit its own thermal expansion. A large quantity of fluid, represented initially by, perhaps, a single GaPH particle, will expand (and birth new particles) into a vacuum via the kinetic effusion process without any need for a mesh. Properly formulated there is no need to do a pressure gradient calculation on the mesh. Pressure effects can now be expressed in either of two ways: (1) kinetic particle flux, as in

PIC, or (2) each GaPH particle undergoes kinetic effusion and births new particles in all directions with finite expansion velocity.

C. *The Evolution of GaPH from Hydrodynamics*

In more familiar terms to practitioners of hydrodynamics, consider a fluid represented on an orthogonal grid on which number density ρ, drift $\mathbf{v}$, and pressure tensor are known at cell centers. Simplifying the pressure tensor by dropping off-diagonal terms leaves the pressure tensor with the thermal energy along each direction E_i. The density and thermal energy E_i are required to be uniform throughout a cell at the beginning of a time step t and at the end $t + \Delta t$. We add the slope of the drift $dv_i/dx_i = 2\mathrm{S}_i/\mathrm{W}_i$ as an additional cell parameter, where S_i is the velocity spread and W_i is the width of a cell. These cell parameters, coupled with the location of the cell, are precisely the parameters that describe a GaPH FSP at an instant in time when the FSP is collocated with a cell.

We select a procedure similar to the Godunov scheme [4] to advance the fluid in time. Like Godunov, our scheme assumes a step discontinuity across a cell boundary and then tracks the evolution of this discontinuity to determine the average flow through that boundary. The results from the net flow and original cell parameters are then fit to the distribution function described by ρ, $\mathbf{v}$, E_i, and S_i. This process completes the evolution of the fluid through a time step Δt. The fitting operation, in fact, constitutes "closure" to the moment equations—an assumption, in this context, which ignores higher moment information.

Our hydrodynamics is now extended to make it more Boltzmann-like through the following steps. First, we extend the hydrodynamics to multiple fluids such that each fluid has an independent mesh and may spatially overlap with other fluids. Birthing of these new independent fluid species, and their associated independent mesh, occur at the beginning of each time step t. This birthing process involves the formation of a new fluid and mesh for each occupied cell. For example, a mesh of $10 \times 10 \times 10$ cells with uniform fill will be restructured such that there are 1000 fluids, each fluid has its own copy of the mesh with one occupied cell and 999 vacuum cells. Coupling between fluids is accomplished through collision terms and other possibly grid-based forces (perhaps an electromagnetic Lorentz force). To this point we have a multifluid code that aggressively births fluids which evolve via advection through cell boundaries. Closure of the moments is provided from the assumed local velocity distribution that will eventually become a "GaPH" particle. This procedure is a first step towards Boltzmann-like behavior because it allows multiple Maxwallian distributions at a single point in space.

At this point we have the opportunity to significantly improve the performance of this algorithm. We can generalize the capabilities of each mesh by allowing its boundaries to move—an arbitrary Lagrangian Eulerian (ALE) concept. For example, we may move the mesh with the center of mass of its occupied cell. This new feature would then reduce the advection problem since each mesh now drifts along with the Lagrangian coordinates of its center of mass.

Merging of these independent fluid species occurs at the end of a time step $t + \Delta t$. This process involves finding pairs of fluids that occupy similar cell location and parameter space, and combining them to form a single fluid. "Similar" requires that merging does not alter salient features of the superposition of fluids. For example, if two fluids "*a*" and "*b*" occupy the same physical space and differ only in the number density, the two fluids are merged such that the new fluid has the sum of the pair's particle number density. In this example

no macroscopic features have been changed and economy has been achieved by converting two fluids into one.

In the final step to GaPH, we change the way cell information is stored. Instead of tracking a mesh for each fluid, each fluid now carried its own spatial extent and location. Mesh details are no longer needed. The adjustment and addition of mesh boundaries, introduced for closure of the moment equations, are made for optimal fluid evolution, again the ALE concept of mesh optimization. In addition, since the new cells will become new fluids at the beginning of the next time step, storage can be allocated as if they were new fluids or, now, simply new fluid element particles with finite size. Details of this final step are discussed in Section III.

D. *The Evolution of GaPH from PIC*

Each GaPH particle contains a given number of real particles per simulation particle N, three positions **x** and three velocity **v** components. As with PIC we could use an ensemble of such particles to statistically reconstruct a distribution function in both space and velocity. In addition each GaPH particle has a finite volume with orthogonal widths of W_1, W_2, and W_3 that enclose the N real particles. These FSPs may also overlap spatially and they certainly do in velocity.

At each spatial position within each GaPH FSP, there exists a full Maxwellian distribution in velocity space. The net distribution function f now consists of the superposition of these individual Maxwellian distributions. Additionally we find empirically that adding an internal velocity slope $dv/dx = 2S/W$, characterized by the velocity spread S_i, greatly reduces the number of particles required to recover the details distributions made through superposition. In multidimensions the internal velocity structure within a GaPH particle is given by the product of the components

$$f(\mathbf{x},\mathbf{v}) = \mathrm{N}\prod_{i=1}^{3}\begin{cases} 0 & \text{if } +\frac{\mathrm{W}_i}{2} < x_i - \mathrm{x}_i, \\ \frac{1}{\mathrm{W}_i\sqrt{\frac{4\pi \mathrm{E}_i}{\mathrm{m}}}}\exp\left(-\frac{\left[v_i-\mathrm{v}_i-(x_i-\mathrm{x}_i)\frac{2\mathrm{S}_i}{\mathrm{W}_i}\right]^2}{\frac{4\mathrm{E}_i}{\mathrm{m}}}\right) & \text{if } +\frac{\mathrm{W}_i}{2} \geq x_i - \mathrm{x}_i \geq -\frac{\mathrm{W}_i}{2}, \\ 0 & \text{if } x_i - \mathrm{x}_i < -\frac{\mathrm{W}_i}{2}, \end{cases}$$

where m is the real particle mass, W_i is the particle width in each direction, and E_i is the thermal energy associated with each direction.

By generalizing the function of each particle, we have added a considerable amount of redundancy to our ability to represent distribution functions. For example, consider a uniform block of gas. In the GaPH representation we can construct this block from a single FSP with the appropriate temperature or a set of smaller overlapping FSPs. This versatility in representing the same distribution provides the redundancy that we exploit when merging particles.

What we have described to this point is largely a PIC algorithm enhanced with "smarter" particles. The hydrodynamic influence appears at this point in the algorithm when we allow each GaPH FSP to expand and birth new particles. During a finite time step Δt, the distribution within each GaPH particle will evolve. There is an exact analytic solution for this expansion in the collisionless case (and, for future work, a reasonable approximation exists for the collisional case). This kinetic effusion solution is described in detail in Section III. By analogy, each GaPH particle, at the beginning of a time step, can be thought of as a sugar

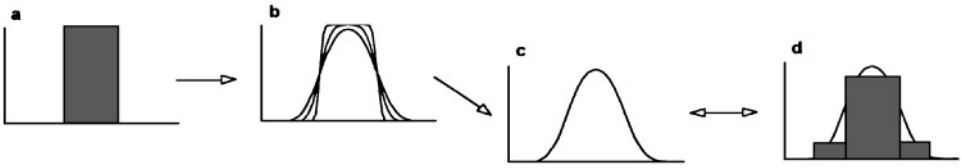

FIG. 1. (a) Initial density profile of GaPH FSP. (b) Snapshots of the evolutionary sequence of the density profile. (c) Evolved density profile. (d) Fit of new GaPH FSP to evolved density profile.

cube of uniform density across its finite size. During the course of the time step, an analytic expression derived from an integral over velocity describes the effusion of real particles out the edges of the GaPH FSP. Clearly, the right going real particles near the right edge of the FSP effuse through the right edge of the GaPH particle; only the fastest particles from positions nearer the left side leave the right edge. The result is that the GaPH particle melts like a sugar cube, shoulders first, then ultimately turning into a melting profile, as in Figs. 1b and 1c.

As soon as the degree to which the GaPH particle "melts" is established, an algorithm to birth new particles is applied. This algorithm consists of finding the best fit for (in this case) three GaPH particles whose internal attributes are determined by such constraints as conservation of energy, momentum, and others. (Exact details are given in Section III.) This process is shown symbolically in Figs. 1c and 1d. The process of fitting the expanded particle with multiple particles results in lost information. This is analogous to closing the moment equations for a hydrodynamic solution. In some sense, fitting to more particles corresponds to closing the system at increased order in the moment equations. It is important to note that even fitting with just three particles results in the number of GaPH particles growing by a factor of 3 every time step—resulting in an astronomical data issue.

GaPH's approach to this explosion of simulation particles is to merge them. In adding internal velocity structure to individual simulation particles, we have added redundancy to our representation. While the distribution function is unique, there is a huge variety of configurations of GaPH particles that can adequately reproduce it. For economy, we exploit this freedom to model with one particle the behavior of many. Through careful comparison, pairs of GaPH particles are selected and merged without losing salient features. The details of this process are obviously critical to the success of GaPH and are discussed in Section IV.

As an example of the physics we wish to address with this method, consider a collision-free expansion of two parallel slabs of gas through one another. Figure 2a depicts the closed form solution of the density profile (the log of the main plot is shown in the upper right). The interpenetration region between the two slabs is certain to have a non-Maxwellian velocity profile from the asymmetric flows.

The dashed curve in Fig. 2b shows a PIC solution. This noisy solution (with an average of 2.5 particles-per-cell) had difficulty recovering the quarter size peak in the distribution. Our GaPH solution is the solid curve in Fig. 2b. As can be seen from the log plots in the upper right-hand corners, the GaPH solution recovers nearly four orders of magnitude of the analytic solution with the same number of particles as PIC. We find that GaPH used relatively few, large particles to form the core of the distribution while smaller particles describe the details at the tails.

Using particle trajectories without the influence of any forces is a contrived way to make a point. That point is that particle codes are often used in situations where poor statistics

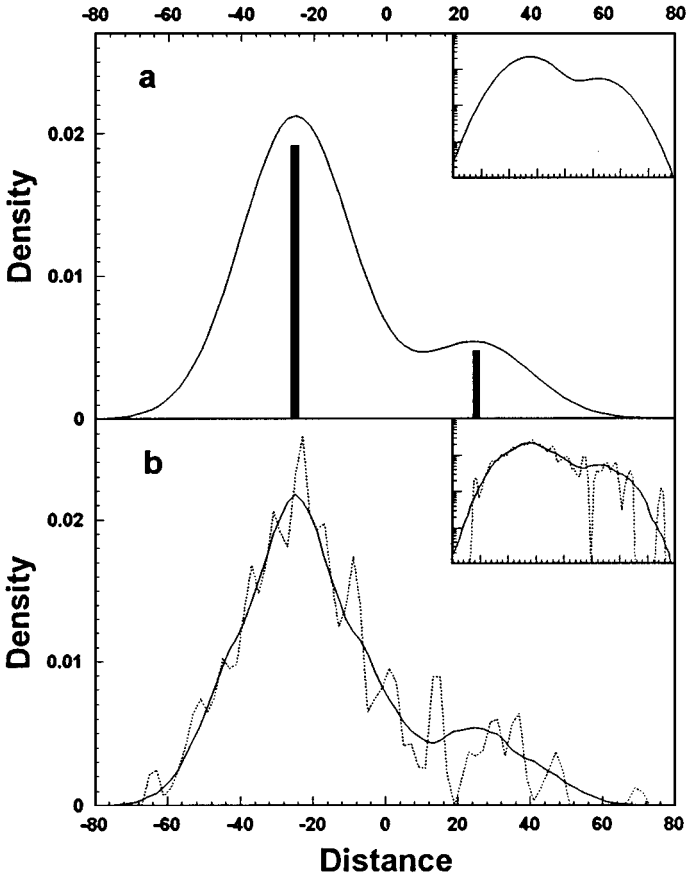

FIG. 2. An analytic solution of the free expansion of two unequal neutral gas puffs through one another. In (a), the bars give position and relative size of the initial distribution. The solid curve is the closed form solution with the corresponding log plot shown in the upper right. In (b), the dashed curve is the result of a collisionless particle solution with 203 particles. The solid curve is the GaPH solution that grew from a two-particle initialization to a final representation with 203 particles. Note that the GaPH and particle solution were both linearly interpolated to the same 80 cell mesh.

guarantee noisy results. If a particle in a PIC calculation wanders into a cell, what exactly can be said about the distribution in that cell? If a GaPH particle wanders into a cell considerably more information is available from its internal structure. What is not contrived is the economic advantage gained by aggressive merging and birthing of freely moving, FSP, fluid "elements."

III. PARTICLE HYDRODYNAMICS: FORMING NEW PARTICLES

Each GaPH particle carries a base set of attributes for hydrodynamics: the mass per real particle m, number of real particles N in each simulation particle of width W_i, position **x**, drift **v**, velocity spread S_i, and thermal energy per-real-particle along eachaxis E_i. In the present formulation, real particle number and thermal energy are distributed uniformly throughout each FSP's volume. Position and drift are assigned at the center of mass and the velocity spread is a linear profile imposed within the volume. To develop the hydrodynamic portion of the algorithm, consider a collision-free distribution contained within a uniform

slab which extends from $-\mathrm{W}/2$ to $+\mathrm{W}/2$. At time $t=0$ the contents within the slab are synonymous with a single "parent" GaPH particle, which has the distribution

$$f(x,v)=\begin{cases}0, & \text{if } -\frac{\mathrm{W}}{2}>x\\ \frac{\mathrm{N}}{\mathrm{W}\sqrt{4\pi\mathrm{E/m}}}\exp\left(-\frac{\left[v-\mathrm{v}-x\frac{2\mathrm{S}}{\mathrm{W}}\right]^2}{4\mathrm{E/m}}\right), & \text{if } -\frac{\mathrm{W}}{2}\le x\le+\frac{\mathrm{W}}{2}\\ 0, & \text{if } x>+\frac{\mathrm{W}}{2}.\end{cases}$$

If the ends of the slab are removed, the density profile for this particle

$$\rho(\mathbf{x},t)=\frac{1}{t}\int_{-\mathrm{W}/2}^{+\mathrm{W}/2}f\left(x,\frac{\mathbf{x}-x}{t}\right)dx=\frac{\mathrm{N}}{2(\mathrm{W}+2t\mathrm{S})}\left[\begin{array}{c}\mathrm{erf}\left(\frac{\mathbf{x}-t\mathrm{v}+\frac{\mathrm{W}}{2}\left(1+\frac{2t\mathrm{S}}{\mathrm{W}}\right)}{\sqrt{4t^2\mathrm{E/m}}}\right)\\ -\mathrm{erf}\left(\frac{\mathbf{x}-t\mathrm{v}-\frac{\mathrm{W}}{2}\left(1+\frac{2t\mathrm{S}}{\mathrm{W}}\right)}{\sqrt{4t^2\mathrm{E/m}}}\right)\end{array}\right] \tag{1}$$

$$v=\frac{\mathbf{x}-x}{t}$$

evolves as mass from each location x within the parent distribution $f(x,v)$ expands to contribute to all locations $\mathbf{x}$ at time t. In a similar manner we track the momentum and energy of the parent's distribution.

$$\mathrm{p}(\mathbf{x},t)=\frac{\mathrm{m}}{t}\int_{-\mathrm{W}/2}^{+\mathrm{W}/2}\left(\frac{\mathbf{x}-x}{t}\right)f\left(x,\frac{\mathbf{x}-x}{t}\right)dx \tag{2}$$

$$\mathrm{e}_{\parallel}(\mathbf{x},t)=\frac{\mathrm{m}}{2t}\int_{-\mathrm{W}/2}^{+\mathrm{W}/2}\left(\frac{\mathbf{x}-x}{t}\right)^2f\left(x,\frac{\mathbf{x}-x}{t}\right)dx \tag{3}$$

$$\mathrm{e}_{\perp}(\mathbf{x},t)=\frac{1}{t}\int_{-\mathrm{W}/2}^{+\mathrm{W}/2}\mathrm{E}_{\perp}f\left(x,\frac{\mathbf{x}-x}{t}\right)dx. \tag{4}$$

At time t, the "parent" particle's evolution is broken up into three "child" particles, a central and two expansion particles. Figure 3 gives a visual depiction of the hydrodynamic evolution of the density and the density fit. The central particle is constructed from the moments of the distribution that remained within the parent volume W. As a result of this assumption, the mass per real particle, center of mass, drift, and thermal energy perpendicular to the direction of expansion transfer to the central particle with little effort. The

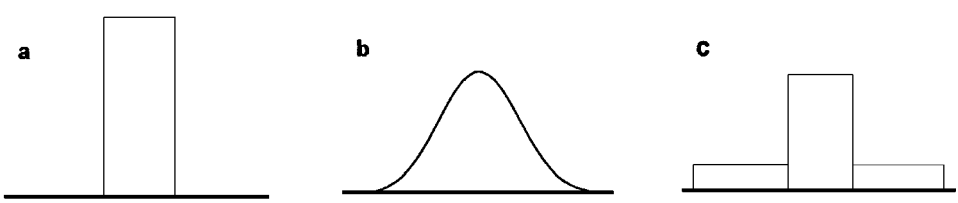

FIG. 3. (a) The density profile at $t=0$. (b) The solution for the evolved density profile at time t. (c) A fit of new particles to the evolved density profile.

relationships are

$$\mathrm{m}_c = \mathrm{m} \tag{5}$$

$$\mathrm{x}_c = t\mathrm{v} \tag{6}$$

$$\mathrm{v}_c = \mathrm{v} \tag{7}$$

$$\mathrm{E}_{\perp c} = \mathrm{E}_{\perp}. \tag{8}$$

Number, velocity spread, and thermal energy can be obtained by fitting to the appropriate velocity moments

$$\mathrm{N}_c = 2\int_{t\mathrm{v}}^{t\mathrm{v}+\mathrm{W}/2} \rho(\mathbf{x}, t)\, d\mathbf{x} \tag{9}$$

$$\triangle \mathrm{v}_c = \frac{2}{\mathrm{m}\mathrm{N}_c}\int_{t\mathrm{v}}^{t\mathrm{v}+\mathrm{W}/2} \mathrm{p}(\mathbf{x}, t)\, d\mathbf{x} \tag{10}$$

$$\mathrm{E} = \frac{2}{\mathrm{N}_c}\int_{t\mathrm{v}}^{t\mathrm{v}+\mathrm{W}/2} \mathrm{e}_{\parallel}(\mathbf{x}, t)\, d\mathbf{x} - \mathrm{m}\left(\frac{1}{2}\mathrm{v}_c^2 + \frac{1}{6}\mathrm{S}_c^2\right), \tag{11}$$

where the second term on the right-hand side of Eq. (11) contains the energy from drift and velocity spread. Finally we need an equation to determine the central particle's volume W_c. Of many options, one that works well is the conservation of second spatial moment about the center of mass,

$$\int_{\mathrm{x}_c-\mathrm{W}_c/2}^{\mathrm{x}_c+\mathrm{W}_c/2} \frac{\mathrm{N}_c}{\mathrm{W}_c}(\mathbf{x}-\mathrm{x}_c)^2\, d\mathbf{x} = 2\int_{t\mathrm{v}}^{t\mathrm{v}+\mathrm{W}/2} (\mathbf{x}-\mathrm{x}_c)^2 \rho(\mathbf{x}, t)\, d\mathbf{x}. \tag{12}$$

To summarize, the central particle's fluid quantities are determined by conserving moments that remain within the original parent's volume.

Expansion particles are formed in much the same way as the central particle, with a few caveats. Each expansion particle is butted up against the central volume, the moment integration is over all space outside the original parent's volume, and the velocity profile is chosen to be continuous. The right expansion particle is characterized by

$$\mathrm{m}_R = \mathrm{m} \tag{13}$$

$$\mathrm{E}_{\perp R} = \mathrm{E}_{\perp} \tag{14}$$

$$\mathrm{N}_R = \int_{t\mathrm{v}+\mathrm{W}/2}^{\infty} \rho(\mathbf{x}, t)\, d\mathbf{x} \tag{15}$$

$$\mathrm{v}_R = \frac{1}{\mathrm{m}\mathrm{N}_R}\int_{t\mathrm{v}+\mathrm{W}/2}^{\infty} \mathrm{p}(\mathbf{x}, t)\, d\mathbf{x} \tag{16}$$

$$\mathrm{S}_R = \mathrm{v}_R - (\mathrm{v}_c + \mathrm{S}_c) \tag{17}$$

$$\mathrm{E}_{\parallel R} = \frac{1}{\mathrm{N}_R}\int_{t\mathrm{v}+\mathrm{W}/2}^{\infty} \mathrm{e}_{\parallel}(\mathbf{x}, t)\, d\mathbf{x} - \mathrm{m}\left(\frac{1}{2}\mathrm{v}_R^2 + \frac{1}{6}\mathrm{S}_R^2\right) \tag{18}$$

$$\int_{\mathrm{x}_c+\mathrm{W}_c/2}^{\mathrm{x}_c+\mathrm{W}_c/2+\triangle \mathrm{X}_R} \frac{\mathrm{N}_R}{\mathrm{W}_R}(\mathbf{x}-\mathrm{x}_c)^2\, d\mathbf{x} = \alpha\int_{t\mathrm{v}+\mathrm{W}/2}^{\infty} (\mathbf{x}-\mathrm{x}_c)^2 \rho(\mathbf{x}, t)\, d\mathbf{x} \tag{19}$$

$$\mathrm{x}_R = \mathrm{x}_c + \frac{\mathrm{W}_c + \mathrm{W}_R}{2}. \tag{20}$$

The factor of α, on the right-hand side of volume Eq. (19), was empirically determined to be 2. Simply put, scaling the expansion particle's second spatial moment or moment of inertia

by α decreased the number of GaPH particles required to recover a distribution with little to no impact on the result. This factor of α was also carried over to the left expansion particle's volume to maintain the natural symmetries between the fit to left $[-\infty, t\mathrm{v} - \mathrm{W}/2]$ and right $[t\mathrm{v} + \mathrm{W}/2, +\infty]$.

IV. MERGING PARTICLES

Determining which pairs of particles are merged to form new particles begins by finding a composite overlap of each pair within the entire system. Finding these composite overlaps requires the product of several tests that compare various components of the pair's parameter space to an ideal case. The first test

$$O_x = \begin{cases} 1, & \text{if } \{a, b\} \text{ spatially overlap,} \\ 0, & \text{if } \{a, b\} \text{ do not spatially overlap,} \end{cases} \tag{21}$$

requires that the particles physically overlap. This ensures the spatial continuity of the particles being merged. The second test compares the density in the spatially overlapping region to the merged density. Ideally there would be no difference between the merged density and the sum of the separate densities. Any deviation from this ideal is considered an error as expressed by

$$\rho_{\mathrm{err}} = \frac{\mathrm{W}}{\mathrm{N}}\left(\frac{\mathrm{N}_a}{\mathrm{W}_a} + \frac{\mathrm{N}_b}{\mathrm{W}_b}\right) - 1. \tag{22}$$

The second factor in the composite overlap, given by

$$O_\rho = \max\left(1 - \left[\frac{\rho_{\mathrm{err}}^2}{S_\rho}\right]^2, 0\right), \quad 0 < S_\rho \leq 1, \tag{23}$$

uses a scaling factor S_ρ to clip unacceptable errors in the density. Typical values for S_ρ range from 0.05 to 0.15. The third test seeks to find what portion of the velocity profile is not represented in the merged particle and whether hydrodynamics will recover the oversight. The error is limited with

$$\begin{aligned} O_{\mathrm{v}} &= \max\left(1 - \frac{\mathrm{m}\mathrm{v}_{os}^2}{\mathrm{E}_\parallel S_{\mathrm{v}}}, 0\right), \quad 0 < S_{\mathrm{v}} \leq \frac{\pi}{4}, \\ \mathrm{v}_{os} &= \max\begin{pmatrix} \max\left(\mathrm{v}_a + \frac{\mathrm{S}_a}{2}, \mathrm{v}_b + \frac{\mathrm{S}_b}{2}\right) - \left(\mathrm{v} + \frac{\mathrm{S}}{2}\right) \\ \left(\mathrm{v} - \frac{\mathrm{S}}{2}\right) - \min\left(\mathrm{v}_a - \frac{\mathrm{S}_a}{2}, \mathrm{v}_b - \frac{\mathrm{S}_b}{2}\right) \\ 0 \end{pmatrix}, \end{aligned} \tag{24}$$

where typical values for S_{v} are $\pi/8$ to $\pi/4$. The fourth and final test compares the spread in thermal energy between the pair and whether the spread can be covered by the ensuing hydrodynamics. We limit the difference in thermal energy by

$$\begin{aligned} O_{\mathrm{T}\parallel} &= \max\left(1 - \left[\frac{\Delta \mathrm{E}_\parallel}{\mathrm{E}_\parallel S_{\mathrm{T}\parallel}}\right]^2, 0\right), \quad 0 < S_{\mathrm{T}\parallel} \leq 1, \\ \triangle \mathrm{E}_\parallel &= \mathrm{E}_{\parallel b} - \mathrm{E}_{\parallel a}, \end{aligned} \tag{25}$$

with typical values for S_{T} of $\sqrt{\pi/8}$ to $\sqrt{\pi/4}$.

Taking the product of the spatial, density, velocity, and thermal energy overlaps gives the composite parameter space overlap. If this number is smaller then a lower limit S_o the overlap is set to zero. This final limit ensures that pairs with multiple marginal overlaps do not merge. Equation (26) gives the composite overlap O_{ab} in parameter space of particle "a" with particle "b" in terms of previously determined overlaps.

$$O_{ab} = \begin{cases} O_{\mathrm{x}} O_{\rho} O_{\mathrm{v}} O_{\mathrm{T}\|} & \text{if } O_{\mathrm{x}} O_{\rho} O_{\mathrm{v}} O_{\mathrm{T}\|} > S_o \\ 0 & \text{if } O_{\mathrm{x}} O_{\rho} O_{\mathrm{v}} O_{\mathrm{T}\|} \leq S_o \end{cases}, \quad 10^{-5} < S_o \leq 10^{-6}. \tag{26}$$

Having obtained these composite overlaps, the maximum overlap $M_{ai} = \max_{a \neq b}(O_{ab})$ is isolated. This means that particle a has its maximum overlap with particle i. If a given pair share the same maximum overlap with each other and that overlap is greater then zero, the pair will be merged. For example, suppose the maximum composite overlap of a with the set $\{b, c, d, e, \ldots\}$ is b. If the maximum net overlap of b, with the set $\{a, c, d, e, \ldots\}$, is a, then the pair will be merged. If, however, the maximum net overlap of b was c, then a will be excluded from merging because the maximum net overlap of a is not symmetric with the maximum net overlap of b. For a social example, particles will *only* marry their favorites; they will remain single rather than settle for second choice. This requirement maintains symmetry; the ordering of the particle set does not effect the outcome.

Once a pair $\{a, b\}$ has been selected for merging, the attributes for the new particle are derived from mass, number, momentum, energy, and moment of inertia conservation. The newly merged particle is defined in terms of the original pair by

$$\mathrm{m} = \frac{\mathrm{m}_a \mathrm{N}_a + \mathrm{m}_b \mathrm{N}_b}{\mathrm{N}_a + \mathrm{N}_b} \tag{27}$$

$$\mathrm{N} = \mathrm{N}_a + \mathrm{N}_b \tag{28}$$

$$\mathrm{x} = \frac{\mathrm{m}_a \mathrm{N}_a \mathrm{x}_a + \mathrm{m}_b \mathrm{N}_b \mathrm{x}_b}{\mathrm{m}_a \mathrm{N}_a + \mathrm{m}_b \mathrm{N}_b} \tag{29}$$

$$\mathrm{v} = \frac{\mathrm{m}_a \mathrm{N}_a \mathrm{v}_a + \mathrm{m}_b \mathrm{N}_b \mathrm{v}_b}{\mathrm{m}_a \mathrm{N}_a + \mathrm{m}_b \mathrm{N}_b} \tag{30}$$

$$\mathrm{S} = \frac{\mathrm{m}_a \mathrm{N}_a \mathrm{S}_a + \mathrm{m}_b \mathrm{N}_b \mathrm{S}_b}{\mathrm{m}_a \mathrm{N}_a + \mathrm{m}_b \mathrm{N}_b} \tag{31}$$

$$\mathrm{E}_{\perp} = \frac{\mathrm{N}_a \mathrm{E}_{\perp a} + \mathrm{N}_b \mathrm{E}_{\perp b}}{\mathrm{N}_a + \mathrm{N}_b} \tag{32}$$

$$\mathrm{E}_{\|} = \frac{\mathrm{m}_a \mathrm{N}_a \mathrm{m}_b \mathrm{N}_b}{\mathrm{m}_a \mathrm{N}_a + \mathrm{m}_b \mathrm{N}_b} \left(\frac{1}{2} [\mathrm{v}_b - \mathrm{v}_a]^2 + \frac{1}{6} [\mathrm{S}_b - \mathrm{S}_a]^2 \right) + \frac{\mathrm{N}_a \mathrm{E}_{\|a} + \mathrm{N}_b \mathrm{E}_{\|b}}{\mathrm{N}_a + \mathrm{N}_b} \tag{33}$$

$$\mathrm{W}^2 = \frac{12}{\mathrm{m}_a \mathrm{N}_a + \mathrm{m}_b \mathrm{N}_b} \begin{bmatrix} \mathrm{m}_a \mathrm{N}_a \left([\mathrm{x}_a - \mathrm{x}]^2 + \frac{\mathrm{W}_a^2}{12} \right) \\ + \mathrm{m}_b \mathrm{N}_b \left([\mathrm{x}_b - \mathrm{x}]^2 + \frac{\mathrm{W}_b^2}{12} \right) \end{bmatrix}. \tag{34}$$

Once a complete scan of the particle set is made and symmetric maximum composite overlapping pairs are merged, the new and reduced set is then tested to determine if further reduction through merging can be achieved. Iterations continue until the particle set stabilizes.

V. RUN TIME CONSIDERATIONS

The merging process, described above, still fails to control the number of particles within the simulation. It fails in two ways. In the case of free expansion into a vacuum, the effusion and fitting process eventually generates particles with infinitesimal mass in an attempt to recover the leading edge of the expansion—with obvious consequences for the CPU requirements. At the other extreme, in quiescent regions, merging can produce particles whose volumes are large compared to spatial dimensions of interest. To avoid these situations, limits have been placed on the fitting algorithm. If fitting to a single particle while conserving mass, number, and second spatial moment generates a volume larger then the dimension of interest, the fitting is limited to just two particles. This pair of particles is similar to the expansion particle except the moment integrals range from $[-\infty, t\mathrm{v}]$ and $[t\mathrm{v}, +\infty]$ and the second spatial moment is conserved. The failure from infinitesimal mass is handled by fitting the evolved parent to a single particle that conserves the appropriate moments. In cases where both limits are violated, the volume limit takes precedence.

A final issue is the requirement for each particle to be compared with the entire set. The n^2 scaling could slow the algorithm down drastically. By introducing a grid, GaPH spatially sorts the particles allowing the large n^2 problem to be converted into a large set of small n^2 problems. Even with this improvement, the merging algorithm could be expensive. Fortunately, early evidence indicates that large particle numbers will not be a significant problem because of the relatively few GaPH particles needed to recover a distribution.

The big savings, however, are not expected to come from the simple kinetics or hydrodynamics modelling, but rather from the modelling that includes chemistry. For arbitrary distributions, the collision process required to do chemistry correctly is also n^2 and requires the calculation of reaction rates and post reaction scattering. The addition of chemistry adds a considerable amount of work to a simulation. Again, we expect that the large reduction in the number of simulation particles will result in a substantial time savings.

VI. TEST CASES

While we expect chemical processes to be the most demanding in CPU requirements, the collisionless situation is the most demanding in the detail that the algorithm must represent. Collisions generally force the distribution towards a Maxwellian, a direction that GaPH prefers because of particle economy. Consequently, collision-free test cases were selected as first tests to determine how well the GaPH algorithm could recover the appropriate distribution that evolves from a single slab expanding into vacuum. We next consider two neutral slabs expanding through, interpenetrating, one another to test GaPH's ability to merge like particles whose origins provide them with counter-streaming drift velocities. Finally we considered an ensemble of GaPH particles subjected to an external, grid-based, EM force. We have purposely chosen "unusual" initial conditions, such as starting with only one or two GaPH particles, to put enough stress on the algorithm to reveal its strengths and weaknesses.

A. *Single Slab*

Consider a single slab with mass, density, width, and temperature of unity placed at the origin. With a time step of $1/2$ the time it takes the R.M.S. velocity to cross the initial width,

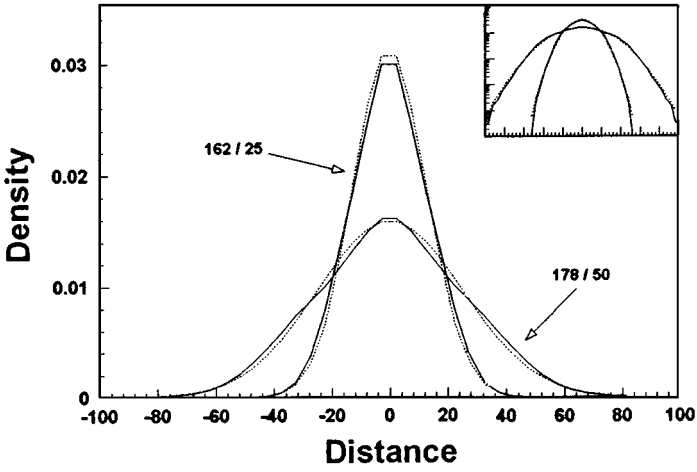

FIG. 4. The solid curve is a GaPH solution that evolved from 1 particle at $x = 0$ to 162 particles in 25 iterations, 178 in 50. The dashed curve is the closed form solution.

the solution is tracked for 50 iterations. Figures 4 and 5 give the density and velocity after 25 and 50 iterations. The similarity between the GaPH solution (solid) and closed form solution (dashed) is remarkable with so few particles, $\sim$200. The error only becomes large in the tails of the distribution which where recovered to four orders of magnitude below the peak. To quantify the error in the density curves after 50 time steps, we plot three forms of the error in Fig. 6. The solid curve gives the relative error compared to the exact solution. The dashed curve demonstrates that the error normalized to the peak of the distribution is always less then 5%. The dotted curve gives the error in terms of the initial profile. Starting with a single particle, the distribution now occupies a volume nearly 100 times its original value—growing in the process to 178 particles. (Were it not for merging and the lower limit on N of 10^{-4}, the system would have been described by 3^{50} particles.) We find that the

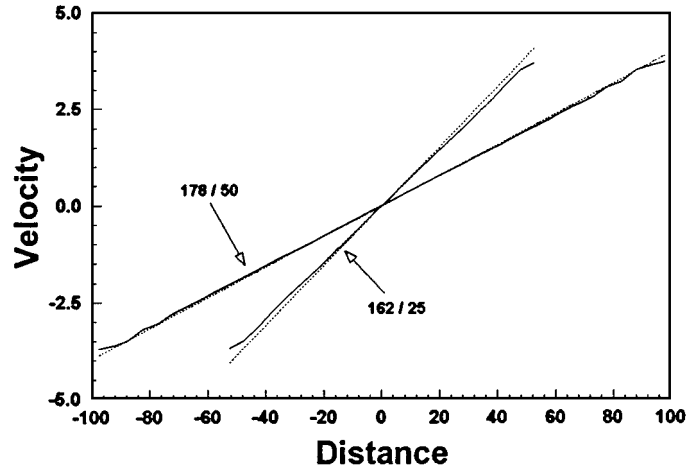

FIG. 5. The solid curve is a GaPH solution that evolved form 1 particle at $x = 0$ to 162 particles in 25 iterations, 178 in 50. The dashed curve is the closed form solution.

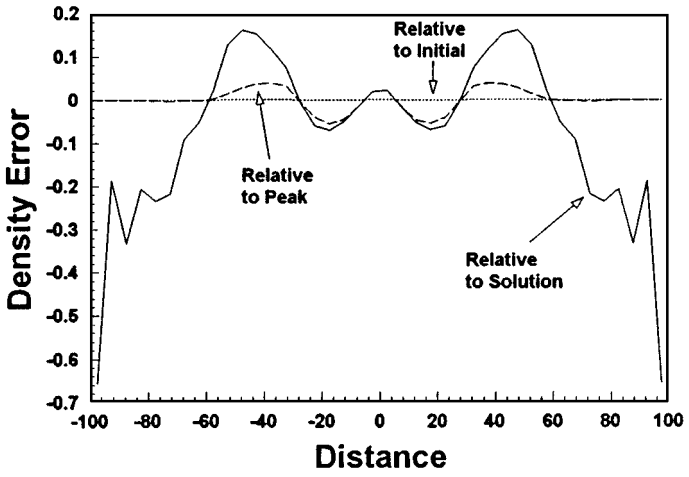

FIG. 6. The error curves for a single slab at 50 iterations are: (GaPH-Actual)/Actual solid curve; (GaPH-Actual)/Current Peak dashed curve; and (GaPH-Actual)/Initial Peak dotted curve.

GaPH solution was never more then 0.2% away from the exact solution when normalized to the initial density.

B. *Symmetric Pair of Slabs*

The next step in characterizing GaPH's capability is to add a second expanding slab. This removes the monotonicity of the first test case and also adds counterstreaming. In this test case two identical slabs, each with half the mass of the single slab in the first case, were positioned at -25.0 and $+25.0$, respectively. The width of each slab was unity, the time step was $1/2$, and the system was tracked over 50 iterations. Figures 7 and 8 give the density and velocity profiles at 25 and 50 iterations. Again the trends of the closed form solution (dashed) are tracked well by GaPH. In this case, however, a noticeable $\sim$6% error can be seen at $x = 0$ for the 25 iteration sampling. But instead of the error persisting, it becomes

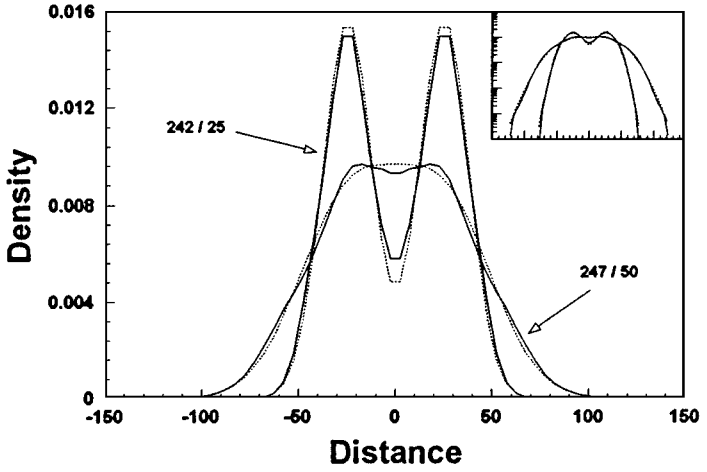

FIG. 7. The solid curve is GaPH solution which evolved form two symmetric particles at $x = -25, +25$, respectively, to 242 particles in 25 iterations, 247 in 50. The dashed curve is closed form solution.

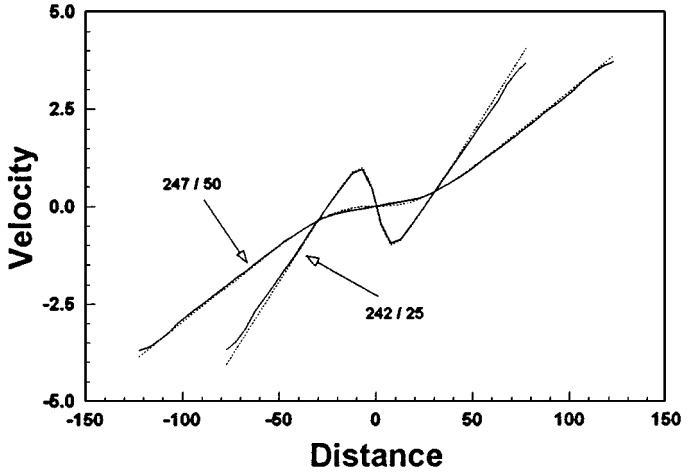

FIG. 8. The solid curve is GaPH solution which evolved form two symmetric particles at $x = -25, +25$, respectively to 242 particles in 25 iterations, 247 in 50. The dashed curve is closed form solution.

insignificant by 50 iterations. The error comes predominantly from the coarse initialization of the system using only two particles. We might characterize the behavior of GaPH as feverishly generating new particles for the first 25 time steps until a reasonable number of simulation particles (for GaPH!) exists to spatially resolve density gradients.

We note that the collision-free cases are the hardest for GaPH to follow. "Wrinkles" in density that are created, say early in the interior due to overlapping of the square edges of new particles, ultimately free-stream to the tails of the distribution. In these regions where the background distribution f is small, the relative error of these early discrepancies become more noticeable. Collisions tend to wash out such problems or, if necessary, more particles could be used in the fit of the evolved particle to ease these relative errors. However, using more particles in the initialization is the most straightforward solution in the present situation. An example of less destructive initial conditions is given in our final test case.

C. *Antisymmetric Slabs*

The first two test cases maintained symmetry about the origin. A test case that breaks this symmetry results if the relative sizes of the previous pair of slabs were adjusted to $2/3$ and $1/3$. Figures 9 and 10 show the density and velocity profiles from GaPH and the exact solution. GaPH tracks the solution well in the presence of this asymmetry—the error associated with the trough has improved—possibly due to the dominance of the left slab over the right.

D. *Step Discontinuity between Large Slabs*

By simply adjusting the size of the two initial particles a completely new type of problem can be modeled. A problem similar to the Riemann problem begins with two adjacent thick slabs, obtained by simply enlarging the finite size of the two previous particles until they touch at $x = 0$. Particle centers are now at $x = -50, +50$ with a width of $W = 100$, and a density of $2/3$ and $1/3$, respectively. As in the previous problems, the mass and temperature are unity and the time step is $1/2$ the time it takes the R.M.S. velocity to cross a unit width.

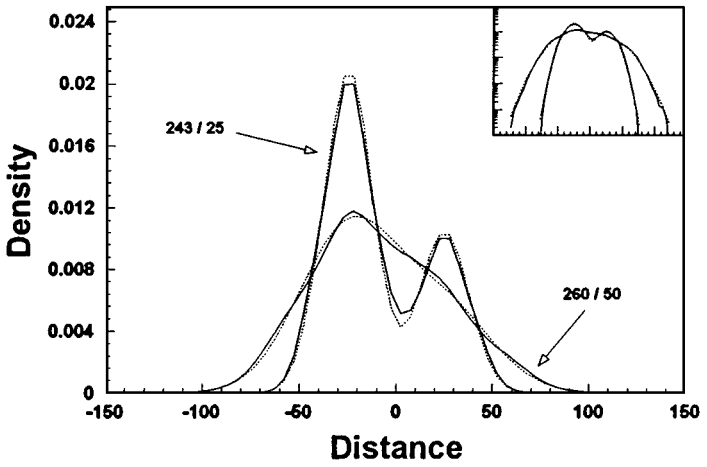

FIG. 9. The solid curve is GaPH solution which evolved form two particles at $x = -25, +25$ with $N = 2/3, 1/3$, respectively, to 243 particles in 25 iterations, 260 in 50. The dashed curve is closed form solution.

Figures 11 and 12 give the evolved distribution after 25 and 50 iterations. Once again GaPH (solid) tracks the solution (dashed) well, but there is a new feature. The GaPH solution oscillates about the exact solution in the neighborhood of the left peak. The origin of the oscillation arises from a run time consideration, in which a limit was placed on the maximum allowed particle volume. For this problem a limit of 10 was imposed. Since the problem began with equal volumes of 100, the first four iterations where spent chopping up the large particles. The hydrodynamic evolution of the ends of the initial particles causes the formation of troughs and peaks. In regions where the ends overlap a peak is observed, where they do not, there is a trough. However, the noise introduced early in the simulation appears to dissipate as the system evolves. It might be expected that a similar problem should occur on the right hand side. The absence of oscillations on the right is a result of particles from the left moving into the region and damping the oscillations.

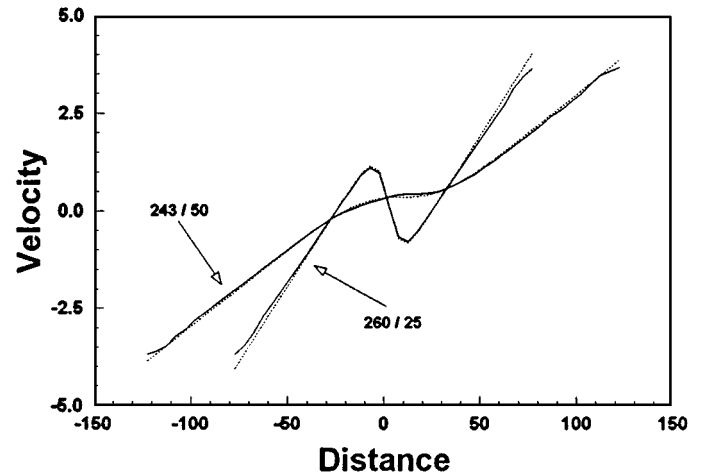

FIG. 10. The solid curve is GaPH solution which evolved form two particles at $x = -25, +25$ with $N = 2/3, 1/3$, respectively, to 243 particles in 25 iterations, 260 in 50. The dashed curve is closed form solution.

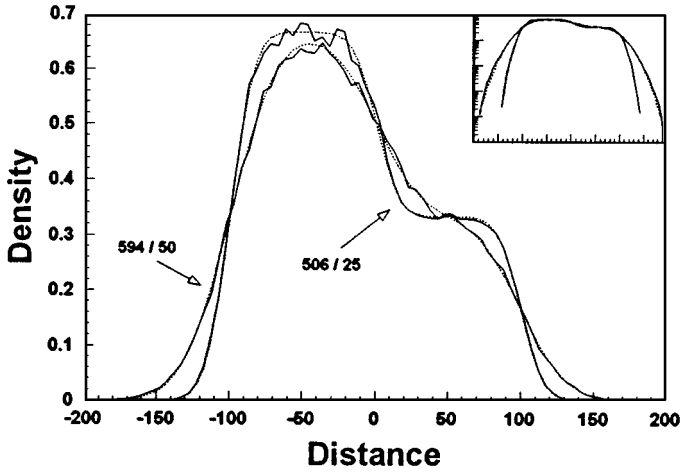

FIG. 11. The solid curve is GaPH solution which evolved form two particles at $x = -50, +50$, W = 100 with N = 200/3, 100/3, respectively, to 506 particles in 25 iterations, 594 in 50. The dashed curve is closed form solution.

E. *Z-Pinch*

Encouraged by these 1D test cases, we have begun to expand the capabilities of GaPH to more practical problems. We have recently combined the GaPH procedure with an electromagnetic fields algorithm based on a zero electron mass Darwin field algorithm [8]. Here a 1D collision-free, Argon z-pinch implosion is presented. Since we have not yet converted the GaPH effusion process to cylindrical geometry, we use a thin shell approximation for each particle. The problem was initialized with 105 evenly spaced, 5.0 eV particles with a uniform density of 10^{12} cm^{-3} form [0.0, 5.0] cm. The current was ramped from zero with a sine function for 75 ns until full current was reached. Taking time steps of 1 ns the system was evolved for 185 ns, stopping before the reflected ion beam crosses the axis. The drift

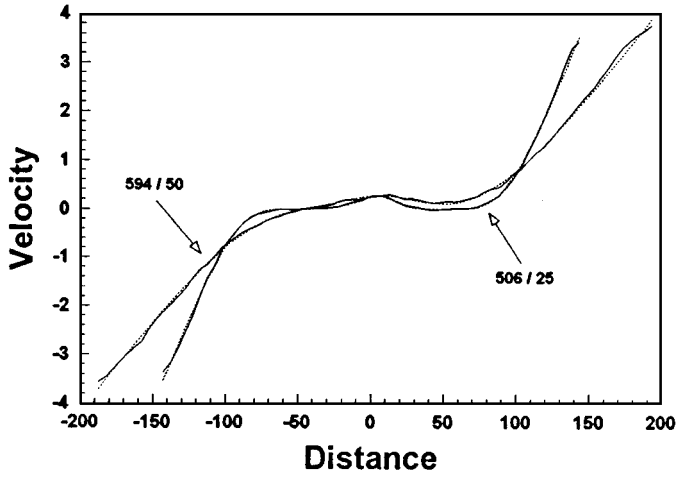

FIG. 12. The solid curve is GaPH solution which evolved form two particles at $x = -50, +50$, W = 100 with N = 200/3, 100/3, respectively, to 506 particles in 25 iterations, 594 in 50. The dashed curve is closed form solution.

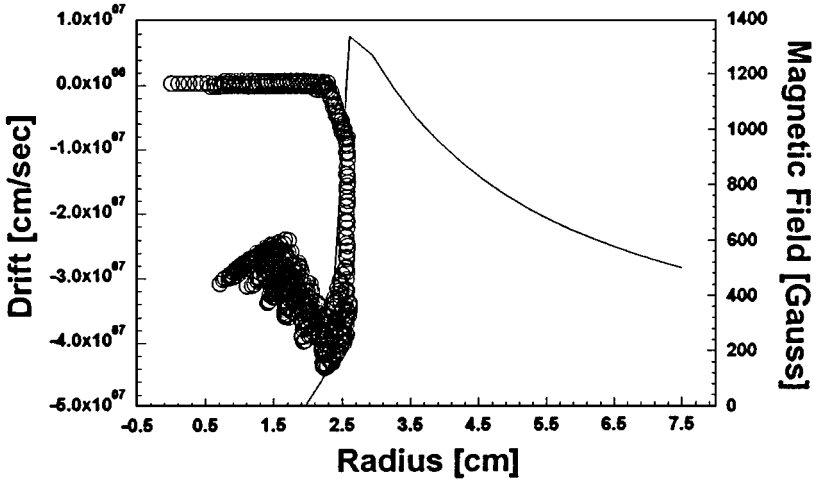

FIG. 13. Ramped current Ar z-pinch that evolved form 105 particles within 5.0 cm to 965 particles over 185 ns to give particle drifts (circles) and magnetic field profile (solid curve).

in the radial direction for each particle, azimuthal magnetic field, and velocity distribution are given in Figs. 13 and 14.

As the azimuthal magnetic field increases, the ions experience an inward force that results in the ion at large radii obtaining a negative radial velocity. As these ions move toward the small radius, the magnetic field grows stronger due to the $1/r$ dependence of this field. The stronger field now causes an even stronger radial force and, as a result, later ions move radially inward with an even larger negative velocity.

There is a feature in the z-pinch simulation which needs to be reconciled. Looking at the particle velocity scatter plots in Fig. 13 there is jitter in the particle drift which narrows as the implosion accelerates inward. This problem with jitter is due to the finite mesh spacing

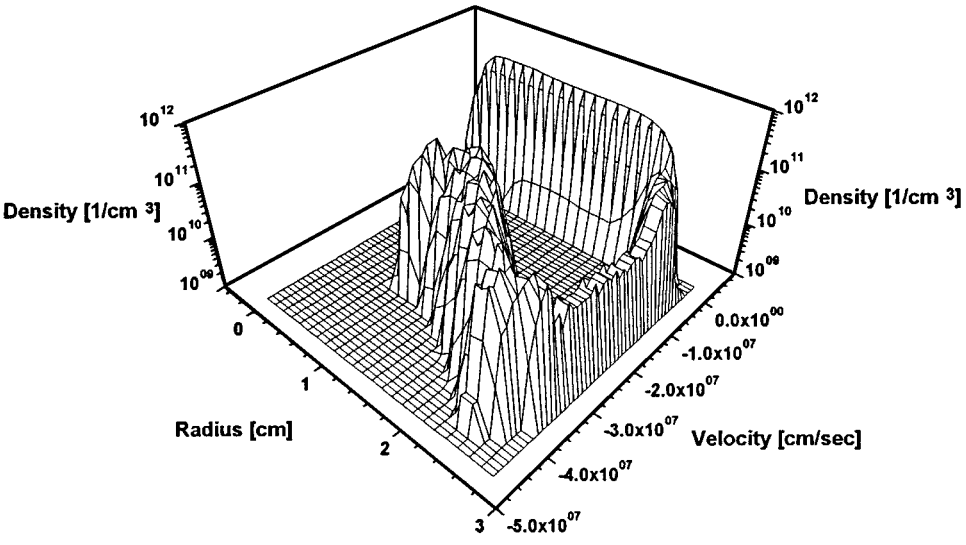

FIG. 14. The velocity distribution of the ramped current Ar z-pinch at 185 ns.

on which the magnetic field is advanced on and the fields are linearly interpolated from. The problem can easily be fixed by a variety of techniques-the simplest being the use of more grid cells!

The jitter points out an interesting feature of GaPH. While the GaPH procedure is not responsible for this behavior, a more aggressive merging algorithm could have smoothed this behavior into a single reflected ion beam. Instead GaPH detected what was considered to be significant "physics" in this counter streaming within the reflected ion beam—and it kept the phenomena. In this case, hindsight suggests the use of more aggressive merging would simplify the result and probably provide better economy.

This case demonstrates that GaPH can be merged with grid based forces, in this case, an electromagnetic field, and that GaPH can successfully detect an emerging bimodal distribution. GaPH accomplishes this without expanding to an unreasonable number of particles.

VII. CONCLUSIONS

We have presented a new type of fluid or plasma transport algorithm called GaPH, or grid and particle hydrodynamics. This algorithm, a combination of the best of PIC and hydrodynamics was intended for applications that are not collisionally dominated, i.e. (for applications in which it matters that the distribution is not a local drifting Maxwellian). Our new procedure uses PIC techniques for its economy in populating only those regions of space that contain particles, for its excellent Lagrangian advection capability, and for its capability to model discontinuous motion in velocity space due to collisions. Our new procedure uses hydrodynamics techniques for its ability to capture a large portion of a distribution with only a few parameters, for its ability to evolve the "GaPH" distribution so that new particles can reasonably probe physical and velocity space, and for the redundancy it added to the superposition of particles.

The combination of PIC and hydrodynamics has resulted in a generalized macro-particle concept so, unlike a simple point particle, each GaPH FSP contains a fluid within itself. The full distribution function is now a superposition of these individual nearly Maxwellian components not simply a superposition of point particles. The internal fluid causes each particle to stretch or effuse in a manner that can accomplish thermal expansion, if necessary, without a computational mesh. After these fluid element FSPs effuse into new shapes, new particles are fit to the evolved shapes in a way that amounts to aggressive birthing of new GaPH particles. These new particles then probe for emerging features. If new features fail to materialize, aggressive merging exploits the redundancy to preserve economy.

The resulting algorithm has proven to be surprisingly effective at recovering the details of particle distributions with a relatively small number of simulation particles. One-dimensional simulations of collisionless expanding slabs have recovered analytic solutions over four orders of magnitude while the volume for the distribution has increased 100 fold. It has accomplished this with only a few hundred particles.

It is this economy of simulation particles that has the promise for affordable, realistic collisionality. We expect collisional physics to be easier than collisionless physics for GaPH. Finally, we have presented a limited first pass of GaPH with a grid based low-frequency electromagnetic field algorithm to learn some of the issues associated with GaPH's treatment of plasma interpenetration in the form of a reflected ion beam in a z-pinch. We are now constructing the collision algorithms that will allow GaPH particles to chemically interact.

Present indications show that, with the addition of collisions, the GaPH algorithm will accomplish its design goal as an economical kinetic simulation model.

REFERENCES

1. D. C. Barnes, T. Kamimura, J.-N. Leboeuf, and T. Tajima, Implicit particle simulation of magnetized plasmas, *J. Comput. Phys.* **52**, 480 (1983).
2. B. M. Marder, GAP-A PIC-type fluid code, in *Math. Comput.* **29**(130), 434 (1975).
3. J. P. Boeuf and E. Marode, A Monte Carlo analysis of an electron swarm in a nonuniform field: The cathode region of a glow discharge in helium, *J. Phys. D* **15**, 2169 (1982).
4. S. K. Godunov, *Mat Sb.* **47**, 271 (1959).
5. G. J. Parker, W. N. G. Hitchon, and J. E. Lawler, Numerical solutions to the Boltzmann equation in cylindrical geometry, *Phys. Rev. E* **50**(4), 3210 (1994).
6. J. J. Monihan, Smooth Particle Hydrodynamics, *Annu. Rev. Astron. Astrophys.* **30**, 543 (1992).
7. G. G. M. Coppa, G. Lapenta, G. Dellapiana, F. Donato, and V. Riccardo, Blob method for kinetic plasma simulation with variable-size particles, *J. Comp. Phys.* **127** (1996).
8. D. W. Hewett, A global method of solving the electron-field equations in a zero-inertial-electron-hybrid plasma simulation code, *J. Comp. Phys.* **38**(3), 378 (1980).